IEEE Access
Multidisciplinary ⋮ Rapid Review ⋮ Open Access Journal

Received 26 March 2024, accepted 9 April 2024, date of publication 15 April 2024, date of current version 26 April 2024.

Digital Object Identifier 10.1109/ACCESS.2024.3389505

RESEARCH ARTICLE

Structural Color in Amber-Entombed Wasp: A Detailed Study Using NS-FDTD Simulations

ZHUO HOU[1], (Member, IEEE), DONGSHENG CAI[2], AND RAN DONG[3], (Member, IEEE)
[1]Graduate School of Systems and Information Engineering, University of Tsukuba, Tsukuba, Ibaraki 305-8577, Japan
[2]Institute of Systems and Information Engineering, University of Tsukuba, Tsukuba, Ibaraki 305-8577, Japan
[3]School of Engineering, Chukyo University, Nagoya, Aichi 470-0393, Japan

Corresponding author: Zhuo Hou (houzhuo.cs1994@gmail.com)

This work was supported by the Japan Science and Technology Agency (JST) Support for Pioneering Research Initiated by the Next Generation (SPRING) under Grant JPMJSP2124.

ABSTRACT The multilayer reflectors of insect epidermis can produce unique structural color through interactions with light. Many fossilized insects, like amber-entombed wasps, present structural colors. However, how this multilayer structure and structural colors are preserved during the fossilization process is still being determined. We use a transfer matrix method (TMM) and a Non-Standard Finite Difference Time Domain (NS-FDTD) simulations to analyze the effects of both expected compressions and expansions of the epidermis layer thickness during fossilization on its structural colors. We estimate the variations of epidermis layer thickness due to the fossilization by measuring their color distances. Surprisingly, we find that the structural coloration of the multilayer reflectors, ranging from blue to green, emitted by many insects remained unchanged from about +5% expansion to -12% compression of their thickness. These findings suggest that, first, insects might have kept their original colors during the fossilization process. Second, the appearance of these structural colors in insects might not just be by chance, but could also be a result of specific evolutionary choices.

INDEX TERMS FDTD, computer graphics, simulation, paleontology, structural color, insects, fossil, optics, photonics.

I. INTRODUCTION

In nature, colors arise from two distinct mechanisms: pigment color and structural color. Pigment color is produced by reflecting light at wavelengths that correspond to the intrinsic color determined by the molecular properties of the substance, resulting in a particular color. On the other hand, physical phenomena such as scattering, diffraction, and interference occur when light is incident on specific nanostructures, resulting in the structural color. The study of biological structural color has a long history, primarily focusing on various insects and feathers [1], [2]. Among these, the multilayer reflector within the epidermis is one of the most common biophotonic nanostructures, producing vivid metallic colors. The study of structural colors has tremendous potential for inferring biological evolution. Recently, McNamara et al. [3] and Kinoshita et al. [4] conducted extensive research on the colors of ancient insects and feathers, providing new methods for the evolutionary deduction of fossil colors and functional evolution. Cai [5] predicted the structural colors of insects with multilayer reflectors using the Transfer Matrix Method (TMM) [6] under the assumption of smooth multilayer films. This study indicates that insects have evolved structural colors around the wavelength of 520nm to improve their survival. However, the paper only discusses the colors of a single structure in terms of wavelength without addressing the changes in the structural color of the wasp's multilayer reflectors within the color space during the compression or expansion of the fossilization. It is important to note that the color space does not directly correspond to the wavelength. Simultaneously, the limitation of this method lies in its reliance on the

The associate editor coordinating the review of this manuscript and approving it for publication was Guido Lombardi.

idealized assumption of smooth multilayer structures, which differ from the irregular rough structures observed under the transmission electron microscope (TEM). To address these issues partly, the Finite Difference Time Domain (FDTD) [7] method is proposed to accurately reproduce the structural color of irregular structures. Musbachet et al. [8] used an FDTD algorithm based on Maxwell's equations to simulate the propagation of electromagnetic waves. This EM simulation-based approach has high accuracy and universality in wave simulations due to its applicability to a wide range of complex structures. Consequently, FDTD method has been applied to the structural color rendering such as Morpho butterflies [9], [10], [11]. Some other rendering methods of structural colors have also been proposed. In addition, McNamara et al. [12] used a 2D Fourier method to reconstruct biological structural colors, whereas this reproduction method only predicts the reflectance of backscattered light and does not consider the viewing angle from the angle of incidence. Evidences [13], [14], [15] have shown that many insects have multilayer reflectors with irregular properties. Additionally, Prum and Torres [16] have demonstrated that this nanostructure was not changed during fossilization and that the multilayer reflectors of insect epidermis can be preserved in fossil insects and amber. We propose to use one of a 2D FDTD simulations to reproduce the original structural color using a rendering pipeline based on Non-standard finite difference time domain(NS-FDTD) [17], [18], [19], [20] method to investigate the structural color detailed in the 2D structures of multilayer reflectors. It's worth noting that the NS-FDTD method is a highly accurate simulation technique, capable of simulating complex optical phenomena, including volume diffraction and interference.

In this paper, we discuss the changes in structural color caused by the compression or expansion of the thickness of the multilayer reflectors. We expect some compression of the multiplayer thickness can occur during the fossilization. The amber-entombed cuckoo wasp, known for its metallic blue-green color as shown in Fig.1, has a typical multilayer reflector that is one of the most common structures in insect structural colorations. The 3D schematic picture of Fig.2(a) demonstrates that the external multilayer structure of an Amber-entombed wasps has a layer array structure with a periodicity about 144 nm. When natural light is incident on the surface of the wasps, the light is reflected or refracted by the multilayer film reflector on the surface and interferes each other resulting in various structural colors. The model design of regular arrangement of the multilayer film structure determines that it can be downscaled to a 1D photonic crystal structure, as shown in Fig.2(b).

The structure of this paper is as follows: In Section II, we introduce the basic principles of the NS-FDTD method. Validation results based on Mie scattering indicate that, compared to analytical method, the NS-FDTD method can provide highly accurate results. In Section III, we employ NS-FDTD simulations to analyze rough multilayer reflectors. We designed simulators for both smooth and rough multilayer

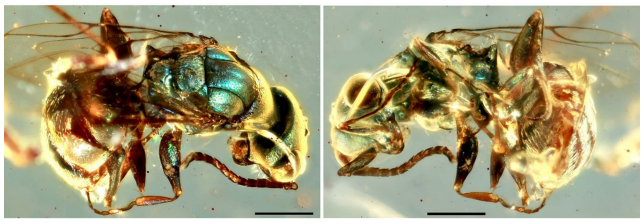

FIGURE 1. Diversified structure color cuckoo wasp photos with bluish-green head, mesosoma and femora. (photo by Cai).

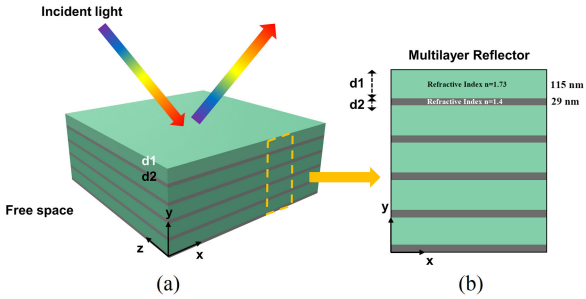

FIGURE 2. (a) Schematic diagram of a 3D model of an insect multilayer reflector. The reflector is a set of regular thin film structures with alternating high and low refractive index layers. (b)Theoretical multilayer mirror modeling the epicuticle of the amber-entombed cuckoo wasp.

reflectors. We simulate the interactions of light with these multilayer reflectors. The structural color mechanism of the multilayer reflectors in fossil insects was analyzed through both theory and simulations. In Section IV, we delve into the details of structural color rendering. We use Near-to-Far Field transformation [21], [22], followed by color transformations to calculate the Bidirectional Reflectance Distribution Function (BRDF) [23], [24], to reproduce the wasp fossil images. In Section V, we initially utilize the Transfer Matrix Method (TMM) to predict the different structural colors corresponding to changes in the thickness of multilayer reflectors. Additionally, leveraging existing images of cuckoo wasps, we measure the color distance between them to provide a comprehensive analysis.

II. NS-FDTD SIMULATOR

Most analyses of multilayer thin-film structures so far have been based on theories or TMM algorithms, which is limited to smooth, parallel perfect multilayer structures. However, the ideal multilayer structures are almost impossible to exist in a real world. Based on TEM images [5], [12], [13], irregular roughness can be observed on the insect's multilayer reflectors. This irregular roughness could generate diffraction, scattering, and other effects, leading to changes in reflectivity and color. Therefore, a high-precision EM wave simulator capable of analyzing complex structures is desired. In this study, we employ the highly accurate Non-standard Finite-Difference Time-Domain (NS-FDTD) method, an optimization of the FDTD method for monochromatic waves, to simulate the rough multilayer reflector

structure. This approach allows us to investigate the complex structural colorations beyond the capabilities of other traditional EM simulations. The FDTD (S-FDTD hereafter) method uses finite differences to approximate spatial and temporal derivatives of Maxwell's equations. For example, the second-order standard finite differences (SFD) for the partial derivatives of a function are given by:

$$\partial_x f(x,t) \cong \frac{\partial_x f(x,t)}{h} = \frac{f(x+\frac{h}{2},t) - f(x-\frac{h}{2},t)}{h} \quad (1)$$

A monochromatic wave can be expressed as:

$$f(x) = e^{i(kx \pm \omega t)} \quad (2)$$

where k is the wavenumber, and ω is the angular frequency. Due to the homogeneous properties of the multilayer thin films structure of the amber-entombed wasp, we can restrict the electromagnetic simulation to a 2-dimensional space. The 2-dimensional simulation space is discretized during the numerical calculation, and the numerical results are dispersed into each grid point $\mathbf{r}(x, y)$ at each discretized time step. Using the above SFDs and space-time discretization, we can derive the S-FDTD method for Maxwell's equations, as:

$$\mathbf{H}(\mathbf{r}, t+\frac{\Delta t}{2}) = \mathbf{H}(\mathbf{r}, t-\frac{\Delta t}{2}) - \frac{\Delta t}{\mu h}\mathbf{d_s} \times \mathbf{E}(\mathbf{r}, t), \quad (3)$$

and

$$\mathbf{E}(\mathbf{r}, t+\Delta t) = \mathbf{E}(\mathbf{r}, t) - \frac{\Delta t}{\epsilon h}\mathbf{d_s} \times \mathbf{H}(\mathbf{r}, t+\frac{\Delta t}{2}), \quad (4)$$

where $\mathbf{E}$, $\mathbf{H}$ represent the electric and magnetic fields, respectively. Here, $\mathbf{d_s}$ is a vectorized differential operator corresponding to $\mathbf{d_s} = (d_x, d_y, 0)$, μ is the permeability, and ϵ is the permittivity. Maxwell's equations are separated into two independent modes in 2-dimensional simulation space: transverse magnetic (TM) and transverse electric (TE) modes. The NS-FDTD method is a more advanced method that improves S-FDTD. In addition, the NS-FDTD method is based on the propagation of monochromatic waves, which significantly improves the accuracy without increasing the computational cost.

In the high-accuracy NS-FDTD method, we replaced the denominator in the SFD with an expression called nonstandard (NS) FD expression:

$$s(k,h) = \frac{sin(\omega \Delta t/2)}{v(x) sin(kh/2)} \quad (5)$$

where $v(x)$ is the wave velocity. The nonstandard finite-difference (NSFDs) for partial derivatives are defined as:

$$\partial_x f(x,t) \cong \frac{\partial_x f(x,t)}{s(k,h)} = \frac{f(x+\frac{h}{2},t) - f(x-\frac{h}{2},t)}{s(k,h)} \quad (6)$$

The NS-FDTD form of the 2-dimensional Maxwell's equations is as follows:

$$\mathbf{H}(\mathbf{r}, t+\frac{\Delta t}{2}) = \mathbf{H}(\mathbf{r}, t-\frac{\Delta t}{2}) - \frac{U_{NS}\mathbf{d_S}}{\sqrt{\mu/\epsilon}} \times \mathbf{E}(\mathbf{r}, t), \quad (7)$$

$$\mathbf{E}(\mathbf{r}, t+\Delta t) = \mathbf{E}(\mathbf{r}, t) - \frac{U_{NS}\mathbf{d_{NS}}}{1/\sqrt{\mu/\epsilon}} \times \mathbf{H}(\mathbf{r}, t+\frac{\Delta t}{2}), \quad (8)$$

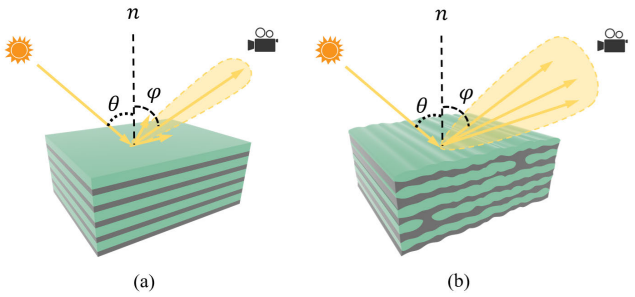

FIGURE 3. Schematic diagrams of (a) an ideal smooth multilayer reflector and (b) a rough multilayer reflector with irregularities.

where $s(k,h) = sin(\omega\Delta t/2)/sin(kh/2)$. In the Non-standard FDTD method, a theoretical error-free high-precision differential operator $\mathbf{d_{NS}}$ is introduced to discretize the Maxwell's equations.

In this study, we construct a multilayer reflector simulator based on the NS-FDTD method. The change in light intensity when irradiated onto the nanostructures of amber-entombed wasps is simulated to determine the potential color mechanism of both ideal and irregular multilayer thin-film structures. The reproduction of structural color is divided into four steps:

- Design the multilayer reflector model based on NS-FDTD method.
- Set up absorption boundary conditions.
- Apply Near-to-Far Field transformation and the color transformation [25] to obtain the Bidirectional Reflectance Distribution Function (BRDF) of the scattering model.
- Apply BRDF constructed in PBRT-V3 render the wasp image using the physically based rendering system [26].

The ideal multilayer reflector, as depicted in the 3D schematic picture in Fig.3, has a periodic stack structure with a thickness of 144 nm. The regular multilayer structure can be simplified into a one-dimensional photonic crystal structure. Observing the TEM image of the amber-entombed wasp, it was found that each multilayer surface possesses irregular protrusions, as shown in Fig.3(b). We model the multilayer surfaces based on the real binary TEM images. When natural light hits the surface of the wasp, the resulting light undergoes small scatterings within the multilayer reflector. The intensity variations of these scattering phenomena are captured at the boundary of the computational domain.

In the NS-FDTD simulation, we adopt an absorbing boundary condition (ABC) [27], where the non-standard ideal matching layer (NS-PML) [28] boundary condition is used in this study. The near-to-far field transformation is applied to transform the transverse magnetic (TM) and transverse electric (TE) near field modes to those of the far field. Finally, a direct angular dependent bidirectional reflectance distribution function (BRDF) is obtained by summing the calculated intensity fields of the two modes.

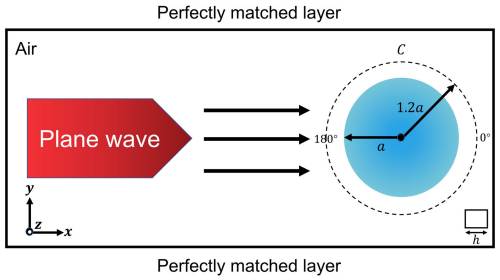

FIGURE 4. Configuration diagram of Mie scattering for validation.

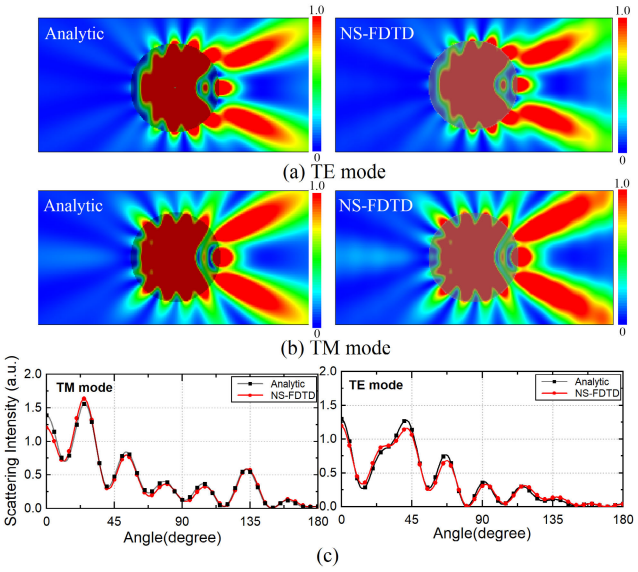

FIGURE 5. Comparison of the analytical results with simulation results in Mie scattering. (a) Intensity spectrum of the analytical and simulation results of Mie scattering in (a) TE mode and (b) TM mode. The color bar on the right side represents the reflected intensity. (c) Comparison of the analytical and simulated results of TE (left) and TM (right) electric field in Mie scatterings.

To validate our NS-FDTD simulator, we compare the numerical solution with the analytical solution for Mie scattering. Mie scattering occurs when the diameter of the particles in the atmosphere is comparable to the wavelength of the radiation. An analytical Mie scattering solution to Maxwell's equations is available for scattering from objects with simple shapes, such as infinitely long cylinders.

In our simulation, a plane wave with a wavelength of 400 nm is irradiated on an infinitely long cylinder with a radius of 400 nm shown in Fig.4. The refractive index of the cylinder is 1.6, and the grid size is 10 nm. We choose the intensity values around the cylinder at distance 1.2 times the radius of the object. Fig.5(a) and (b) show the intensity spectra of the analytical and simulated Mie scattering. Fig.5(c) shows the intensity distribution of the electric field component Ey in TM mode and the scattered intensity of the electric field component Ez in TE mode. The results show that the simulation results agree with the analytical solution of the Mie scattering, and the error of the simulation results is less than 1.5% using a mesh size 10nm × 10nm.

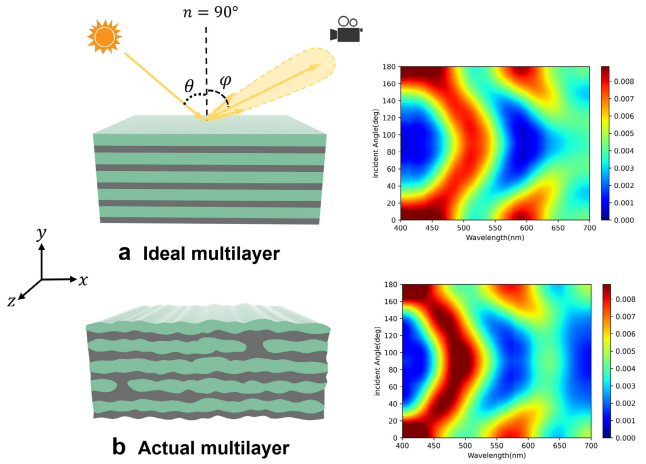

FIGURE 6. (a) The ideal multilayer reflector and its reflection spectrum; and (b) The multilayer reflector with irregularity and its reflection spectrum.

III. ANALYSIS OF MULTILAYER REFLECTOR ON STRUCTURAL COLOR

In this section, we utilize the FDTD method to simulate light propagation in both the smooth and rough multilayer reflectors of the fossil wasp. These allow us to investigate some aspects of the optical properties of the structural colors in fossil wasps. Regarding the multilayer reflector that is the epicuticle of both extant and fossil [5], the total thickness of the cuckoo wasp multilayer reflector is about 770 nm, including five alternating layers. One has a high refractive index of the electron-dense layer with a thickness about 115 nm, and another is a low refractive index of the electron-transparent layer with a thickness about 29 nm. The refractive indices are, respectively, 1.4 and 1.73 for the low and high refractive index layers, and the remaining area is air with a refractive index of 1.0.

We model the multilayer reflector of the amber-entombed cuckoo wasp with irregularities in each layer based on the TEM image in [5]. Next, we simulate the reflection spectrum of this multilayer reflector by NS-FDTD method. We then compare the reflectance spectrum of the smooth multilayer reflector with that with roughness both in surfaces and structures. The refractive index and thickness parameters used for the simulation are the same as those used in TMM (Transfer Matrix Method). Meanwhile, since the magnetic permeability of the multilayer reflector in the epidermis of the fossil wasp is almost the same as that in a vacuum, we set these two models as lossless multilayer films. We binarize the TEM images and implement multiple protrusions and depletions at the junction of each layer to simulate a realistic insect multilayer reflector in the epidermis. In the NS-FDTD simulation solver, to model the realistic multilayer reflector, we determine the thickness of the layers using Gaussian random samplings. The mean value of the random sampled thickness is the thickness of each layer. Since the permeability of the outer skin of the wasp is almost the same as that in a vacuum, we design this reflector model as one with

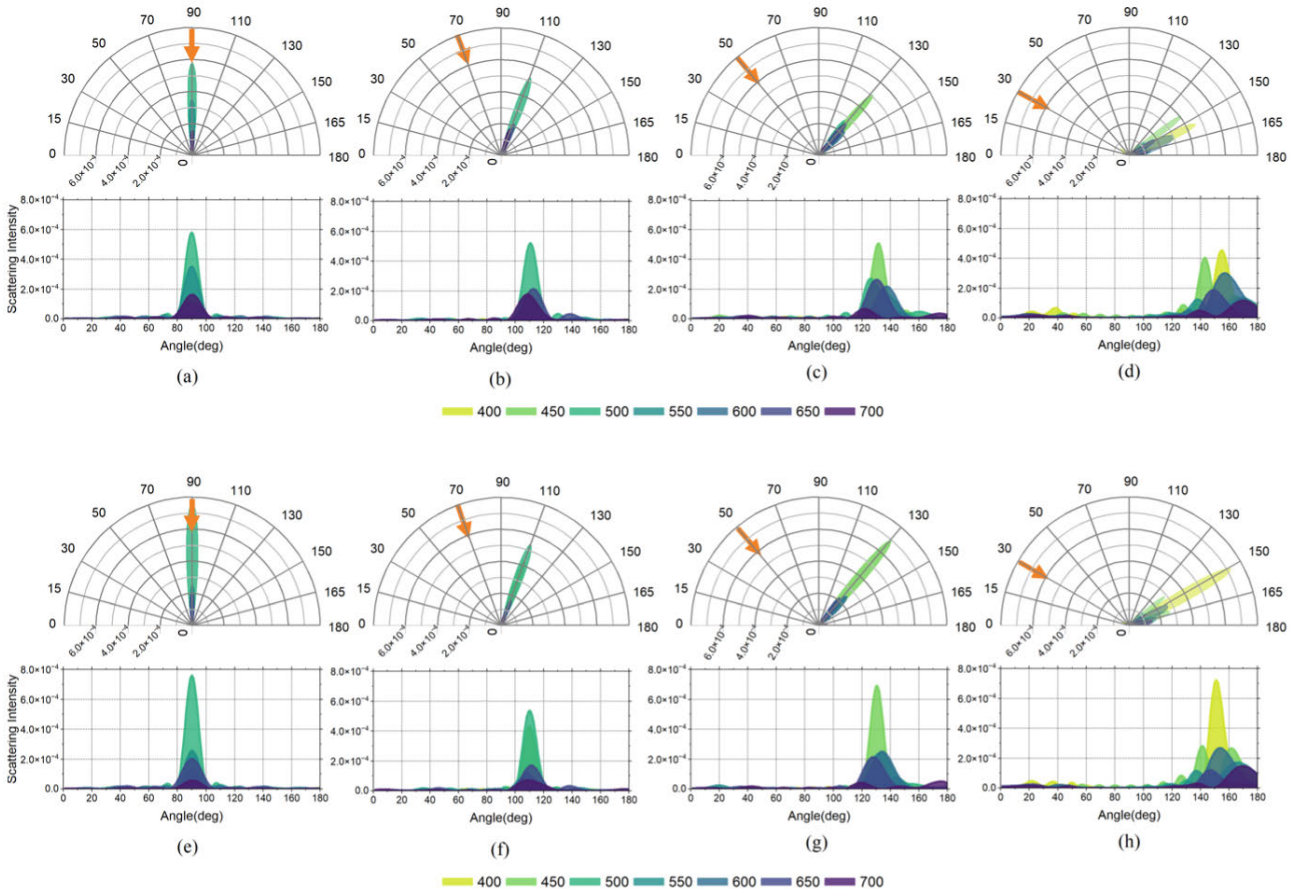

FIGURE 7. Reflection intensity spectrum of the multilayer reflector from different incidence angles of 90, 70, 50, and 30 degrees: (a,b,c,d) for the ideal multilayer reflector and (e,f,g,h) for the rough multilayer reflector with irregularity.

TABLE 1. Simulation parameters for computing amber-entombed wasp reflection intensity.

Parameter	
incident light angle (θ)	0 - 180° (10°increments)
reflection angle (ϕ)	0 - 180° (1°increments)
wavelength	400 - 700 nm (10 nm increments)
grid spacing	10 nm
computational domain	2.5μm × 2.5μm
iteration steps	2000

no additional losses. We generate an infinite set of plane waves propagating along the y-direction and impinging on the multilayer reflector. We calculate the reflection intensity from Transverse magnetic (TM) and Transverse electric (TE) modes at different wavelengths ranging from 400 nm to 700 nm. Each wavelength corresponds to an incidence angle from 0 to 180°, and we set an incidence angle 90° in the vertical direction. The Courant-Friedrichs-Lewy condition determines the model's time step, the grid's spacing is 10 nm, and a 20-layer NS-PML absorption boundary condition is set at the edge of the computational domain. The simulation parameters are listed in Table 1.

According to the reflectance intensity of the ideal multilayer reflector shown in Fig.6(a), the ideal multilayer structure produces strong reflections in the wavelength range from 450 nm to 550 nm at the normal incidence angle $\theta = 90°$. It has a main peak [29] at the wavelength $\lambda = 520$ nm, whereas the slight peak occurs at $\lambda = 600$ nm. The spectral shape of the irregular multilayer reflector shown in the Fig.6(b) is almost the same as that of the ideal multilayer film. However, the results show a significant leftward minus shift about 50-70 nm (shorter wavelength) in the spectrum, with the main peak occurring at $\lambda = 490$ nm, indicating a shift in color towards bluish green at normal incidence angle. This is due to the diffraction and scattering of light caused by the irregularity on the each layer surface in the multilayer reflector. With the increase of the incidence angle from the vertical direction, each peak of the main wavelength are significantly shifted to the left (shorter wavelength).

We calculate the BRDF function of the multilayer reflectors using both the near-to-far transform and the color conversion to CIE XYZ color space. Fig.7 shows the polar plots of the reflection intensity of the two multilayer reflectors at different incidence angles $\theta = 90°$, 70°, 50°, and 30°, which is a part of BRDF. The figure shows the scattered

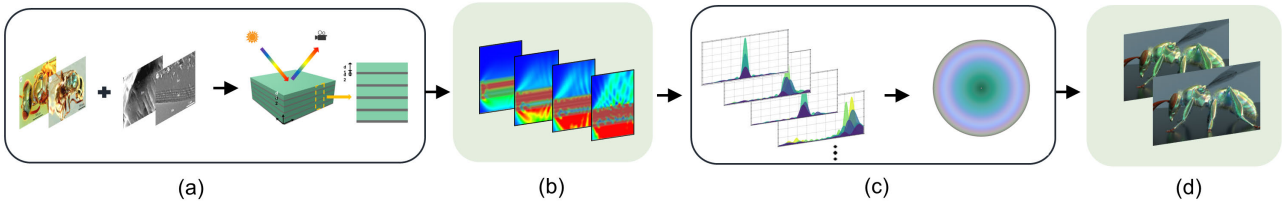

FIGURE 8. Amber-entombed wasp structural color rendering processes: (a) Design a suitable electro- magnetic simulated scattering models based on the nanostructures in 2D image from SEM or TEM. (b) Determine the boundary conditions and light sources for the simulation, and perform multiangle and multi-wavelength electromagnetic simulations using the designed scattering model. (c) Calculate bidirectional reflectance distribution function (BRDF) using the near-to-far field transformation and obtain the rendering texture by color transformation. (d) Design insect 3D models and embed rendering texture into the renderer to reconstruct structural color.

intensity distribution of the incident light at different wavelengths at each reflection angle ϕ (also called the observation angle). The figure shows that for both types of reflectors at different incidence angles, the dominant wavelength is almost the same and shorter. However, compared to the ideal reflector, the intensity of the dominant wavelength in the rough reflector is larger, indicating that the rough reflector has stronger robustness towards shorter wavelengths. In addition, at each incidence angles, the differences between that of the dominant wavelength and other wavelengths is greater, making the dominant color more prominent and brighter. Furthermore, as the incident angle decreases, the dominant wavelength shifts to shorter wavelengths. The figure also show that the reflection of the highlight portion of the multilayer reflector is very close to the specular reflection characteristic, occurring at approximately the same angle as the reflection angle. It is worth noting that some small backscattering also occurs at about the same reflection angle.

IV. REPRODUCING THE FOSSIL STRUCTURAL COLOR

In this section, we reproduce the structural color of an amber-entombed wasp with a typical multilayer reflector based on the pipeline illustrated in Fig.8. We simply implement the Lambertian Reflection method [30] in the PBRT-V3 path tracer, whose BRDF is a constant factor denoted as:

$$f_{Lambert}(\phi, \theta) = \frac{R_{spectrum}}{\pi} \tag{9}$$

The equation includes the incident angle θ and reflection angle ϕ, which corresponds to Fig.6(a). Here, $R_{spectrum}$ denotes either the color texture or the ratio of light reflection to absorption. It also corresponds to the RGB tristimulus values of the texture, obtained through color transformations to the CIE 1931 XYZ color space.

We input the spectral texture table $R_{spectrum}$ into the path tracer for rendering, representing color variations observable from different angles and under varied lighting conditions. As shown in Fig.9, at normal incident angles, the RGB spectral texture distribution illustrates that the ideal multilayer reflector displays a green spectrum at narrower observation angles, whereas the actual reflector exhibits a bluish-green hue. In our rendering model, we assume

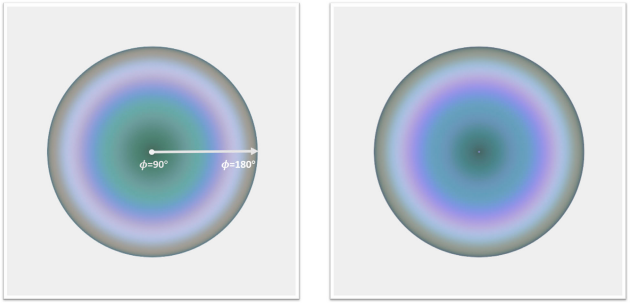

FIGURE 9. Spectral texture color distribution in RGB system at normal incident angles; (a) and (b) are, respectively, spectral color distribution of the ideal and TEM imaged multilayer reflector.

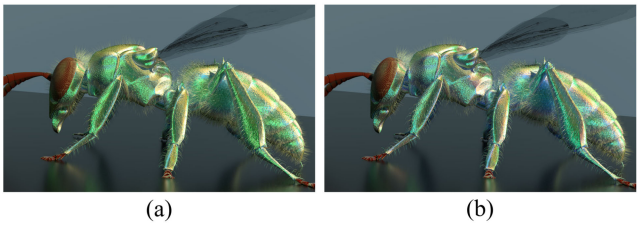

FIGURE 10. Fossil wasp rendering images;(a) green metallic appearance based on the ideal multilayer reflector; and (b) bluish green metallic appearance based on the actual multilayer reflector.

the multilayer reflector is vertically aligned on the insect's surface and use D65 [31] as the standard light source, Fig.10 demonstrates the rendered images from both the ideal and the actual multilayer structures. The results reveal that the ideal multilayer reflector produces a green hue, whereas the actual reflector exhibits a bluer green, closely matching the real wasp colors in Fig.1(a) and Fig.14(a) for a more realistic representation.

V. CHANGES OF MULTILAYER REFLECTOR THICKNESS DUE TO FOSSILIZATION

In this section, we assume that only the thicknesses of the multilayer vary during the fossilization. We use the Transfer Matrix Method (TMM) to discuss the robustness of structural color changes triggered by the compression or

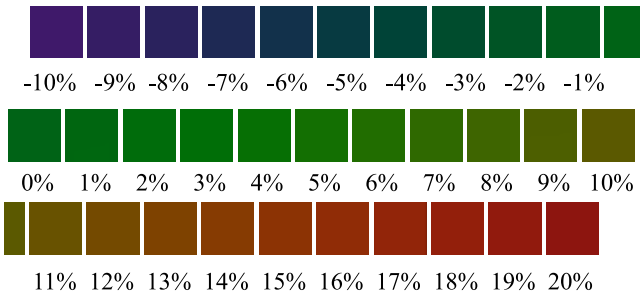

FIGURE 11. Multilayer structural colors calculated using TMM. Negative percentage indicates the compression, and positive percentage indicates the expansion of the multilayer structure.

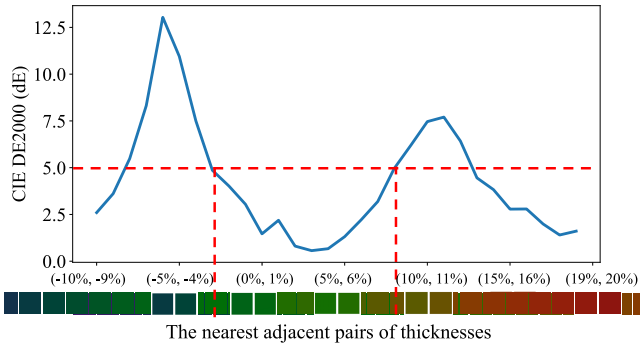

FIGURE 12. Color distance among the compressed/expanded multilayer reflectors is measured using CIE DE2000. The color variations result from the expansion/compression of the reflector and are calculated using TMM.

expansion of the thickness of the multilayer reflectors. Since the primary variable under investigation in this section is the linear compression and expansion of multilayer structure thickness. TMM's computational efficiency allows us to systematically explore a range of thickness variations, providing insights into the physical changes encountered during the fossilization process and their impact on the robustness of structural colors. Although the NS-FDTD method offers higher precision and can simulate more complex structural details, the relative simplicity and computational efficiency of TMM enable us to focus on the key factors influencing the robustness of structural colors during fossilization without the additional computational complexity that NS-FDTD might involve. Here, we expect a certain degree of compression in the multilayer thickness can occur during the fossilization process. The incident angle of the sunlight is set to be vertical in this investigation.

Fig.11 presents the changes in structural colors varying the thickness of the multilayer reflector on the epidermis surface of an amber-entombed cuckoo wasp. In this theoretical calculation, the thickness of this multilayer reflector linearly changes from −10% compression to +20% expansion. Fig.12 is the color distance caused by multilayer thickness expansion/compression. For the color distance metric, the CIE DE 2000 distance is used [32]. Fig.12 indicates the color sensitivity/robustness caused by

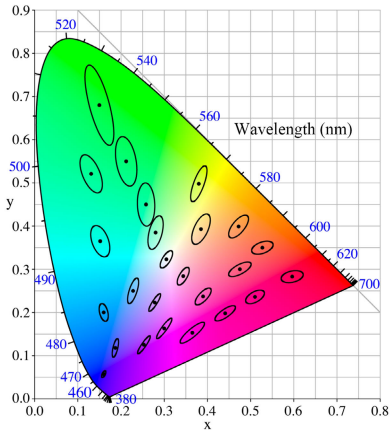

FIGURE 13. Diagram of the MacAdam ellipse.

the thickness expansion/compression. Especially, the low sensitivity/high robustness region indicated as the region less than 5 dE in Fig.12 reveals the color robustness due to expansion/compression of the multilayer thickness in the structural color emitted from the wasp's epidermis for a layer thickness ranging from −4% to 7%. This means the wasp structural color consistently stay within the green spectrum. This robustness implies that changes in the insect's epicuticle thickness within this range, due to compression or expansion during the fossilization process, are relatively insignificant and the insect can preserve almost the same color. However, beyond this range, substantial changes in structural color due to the changes in epicuticle thickness can occur. Therefore, we expect that the structural colors of amber-entombed wasp fossils can preserve the original color within this range of expansion/compression during fossilization.

This robustness of the wasp structural color also can be observed in the MacAdam ellipses [33] as displayed in Fig.13. The MacAdam ellipses is a region on a chromaticity diagram that contains colors that are indistinguishable from the color at the center of the ellipse. The figure shows that the green colors are kept unchanged for the large range of wavelengths from 490 to 560 nm. We also measure the color difference between the extant cuckoo wasp image and the same structural colors from theoretical multilayer reflector in Fig.3, calculated using the same TMM method and the image of one of extant cuckoo wasps shown in Fig.14(a). In the figure, the thickness expands/compresses −10/20%, as demonstrated in Fig 14(b). The origin is the multilayer reflector of the amber-entombed wasp. The x-axis represents thickness changes from −10% to 20%. The y-axis represents the color difference between that of the multilayer reflector and that of the image. The CIE DE2000 color difference between the extant cuckoo wasp and the theoretical model reveals that the color difference initially increases with thickness increase (expansion), then starts to decrease after the thickness expands by 5%, reaching a minimum (21 dE) around the 8% to 9% expansion. Beyond 9%, the color

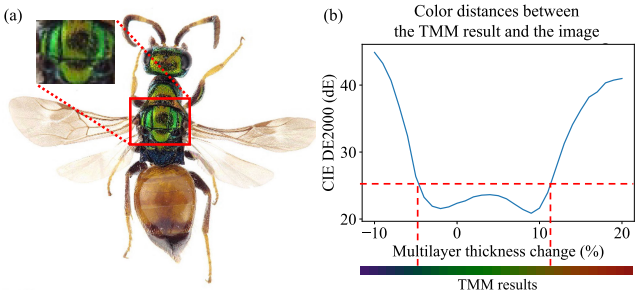

FIGURE 14. Structural color distances between the colors of the specific part in the real wasp photo image and those of theoretical wasp structural color, measured by CIE DE2000.

difference increases largely towards 40 dE. Within the change of −6% to 11% in the figure, the compression or expansion of the multilayer reflector does not significantly alter the color. If we assume that there have been no evolutionary changes in the cuckoo wasp epicuticle multilayer structure, we expect the multilayer thickness may have compressed or expanded within this range during the fossilization.

VI. DISCUSSIONS AND CONCLUSION

In this study, we use the theoretical TMM calculations and the NS-FDTD electromagnetic simulations to estimate the potential changes of the thickness of the multilayer reflector of fossil insects. Insects with metallic bluish green colors may have undergone color changes during fossilization, which possibly coursed by changes in the thickness of the multilayer reflector (compression). In this paper, (1) first, we use TMM to model theoretically and visualize the structural color of the insects, and estimate the impact of changes in the thickness of the insect multilayer reflectors on structural colors; (2) second, regarding to the irregularities in the multilayer reflector, we use the NS-FDTD electromagnetic simulation to obtain the reflection spectrum from the realistic insect multilayer reflector; and (3) finally, we use the physics-based renderer PBRT-v3, and through the rendering pipeline of the NS-FDTD method to reproduce the insect structural color image that can estimate the original colors of the insect. Discussions and conclusions can be summarized as follows:

(1) Our analyses reveal that within the thickness changes ranging from −5% (compression) to 10% (expansion), the color of the multilayer reflector are robust and stay in the green region. Thus, we expect the original colors are preserved during the fossilization if they compress/expand within this range; (2) The irregularities in multilayer structures in roughness and thickness can shift the dominant wavelength to shorter wavelengths, leading to the shift in color from green to bluish green; and (3) Our rendering results reproduce the realistic appearance of the amber-entombed wasp, and this shows the potential and impact of the possible future research on the investigation and reproduction of the structural colors in the fossilized creatures.

ACKNOWLEDGMENT

The authors wish to thank Prof. Cai and Dr. Dong for their great help on research and JST SPRING for providing the necessary support for this research.

REFERENCES

[1] P. Vukusic, J. Sambles, C. Lawrence, and R. Wootton, "Now you see itnow you don't," *Nature*, vol. 410, no. 6824, p. 36, 2001.
[2] P. Vukusic and J. R. Sambles, "Photonic structures in biology," *Nature*, vol. 424, no. 6950, pp. 852–855, Aug. 2003.
[3] M. E. McNamara, D. E. G. Briggs, P. J. Orr, H. Noh, and H. Cao, "The original colours of fossil beetles," *Proc. Roy. Soc. B, Biol. Sci.*, vol. 279, no. 1731, pp. 1114–1121, Mar. 2012.
[4] S. Kinoshita, S. Yoshioka, and J. Miyazaki, "Physics of structural colors," *Rep. Prog. Phys.*, vol. 71, no. 7, Jul. 2008, Art. no. 076401.
[5] C. Cai, E. Tihelka, Y. Pan, Z. Yin, R. Jiang, F. Xia, and D. Huang, "Structural colours in diverse mesozoic insects," *Proc. Roy. Soc. B, Biol. Sci.*, vol. 287, no. 1930, Jul. 2020, Art. no. 20200301.
[6] T. Zhan, X. Shi, Y. Dai, X. Liu, and J. Zi, "Transfer matrix method for optics in graphene layers," *J. Phys., Condens. Matter*, vol. 25, no. 21, May 2013, Art. no. 215301.
[7] K. Yee, "Numerical solution of initial boundary value problems involving Maxwell's equations in isotropic media," *IEEE Trans. Antennas Propag.*, vol. AP-14, no. 3, pp. 302–307, May 1966.
[8] A. Musbach, G. W. Meyer, F. Reitich, and S. H. Oh, "Full wave modelling of light propagation and reflection," *Comput. Graph. Forum*, vol. 32, no. 6, pp. 24–37, Sep. 2013.
[9] D. Zhu, S. Kinoshita, D. Cai, and J. B. Cole, "Investigation of structural colors inMorphobutterflies using the nonstandard-finite-difference time-domain method: Effects of alternately stacked shelves and ridge density," *Phys. Rev. E, Stat. Phys. Plasmas Fluids Relat. Interdiscip. Top.*, vol. 80, no. 5, Nov. 2009, Art. no. 051924.
[10] M. Kambe, D. Zhu, and S. Kinoshita, "Origin of retroreflection from a wing of theMorphoButterfly," *J. Phys. Soc. Jpn.*, vol. 80, no. 5, May 2011, Art. no. 054801.
[11] R. T. Lee and G. S. Smith, "Detailed electromagnetic simulation for the structural color of butterfly wings," *Appl. Opt.*, vol. 48, no. 21, p. 4177, 2009.
[12] M. E. McNamara, D. E. G. Briggs, P. J. Orr, S. Wedmann, H. Noh, and H. Cao, "Fossilized biophotonic nanostructures reveal the original colors of 47-million-year-old moths," *PLoS Biol.*, vol. 9, no. 11, Nov. 2011, Art. no. e1001200.
[13] J. Kroiss, E. Strohm, C. Vandenbem, and J.-P. Vigneron, "An epicuticular multilayer reflector generates the iridescent coloration in chrysidid wasps (Hymenoptera, Chrysididae)," *Naturwissenschaften*, vol. 96, no. 8, pp. 983–986, Aug. 2009.
[14] J. P. Vigneron, M. Rassart, C. Vandenbem, V. Lousse, O. Deparis, L. P. Biró, D. Dedouaire, A. Cornet, and P. Defrance, "Spectral filtering of visible light by the cuticle of metallic woodboring beetles and microfabrication of a matching bioinspired material," *Phys. Rev. E, Stat. Phys. Plasmas Fluids Relat. Interdiscip. Top.*, vol. 73, no. 4, Apr. 2006, Art. no. 041905.
[15] J. Kroi, "Chemical attraction and deception. Intra and interspecific communication in hymenoptera," Ph.D. dissertation, Faculty Natural Sci. III Biol. Preclinical Med., Univ. Regensburg, Regensburg, Germany, 2009.
[16] R. O. Prum, "A Fourier tool for the analysis of coherent light scattering by bio-optical nanostructures," *Integrative Comparative Biol.*, vol. 43, no. 4, pp. 591–602, Aug. 2003.
[17] R. E. Mickens, *Applications of Nonstandard Finite Difference Schemes*. Singapore: World Scientific, 2000.
[18] J. B. Cole, "High-accuracy yee algorithm based on nonstandard finite differences: New developments and verifications," *IEEE Trans. Antennas Propag.*, vol. 50, no. 9, pp. 1185–1191, Sep. 2002.
[19] J. B. Cole and S. Banerjee, "Applications of nonstandard finite difference models to computational electromagnetics," *J. Difference Equ. Appl.*, vol. 9, no. 12, pp. 1099–1112, Dec. 2003.
[20] Z. Hou, D. Cai, and R. Dong, "Photonic rendering for hair cuticles using high accuracy NS-FDTD method," in *Proc. ACM SIGGRAPH Talks*, 2021, pp. 1–2.
[21] R. J. Luebbers, K. S. Kunz, M. Schneider, and F. Hunsberger, "A finite-difference time-domain near zone to far zone transformation (electromagnetic scattering)," *IEEE Trans. Antennas Propag.*, vol. 39, no. 4, pp. 429–433, Apr. 1991.

[22] R. Luebbers, D. Ryan, and J. Beggs, "A two-dimensional time-domain near-zone to far-zone transformation," *IEEE Trans. Antennas Propag.*, vol. 40, no. 7, pp. 848–851, Jul. 1992.
[23] R. L. Cook and K. E. Torrance, "A reflectance model for computer graphics," *ACM SIGGRAPH Comput. Graph.*, vol. 15, no. 3, pp. 307–316, Aug. 1981.
[24] B. T. Phong, "Illumination for computer generated pictures," *Commun. ACM*, vol. 18, no. 6, pp. 311–317, Jun. 1975.
[25] G. Wyszecki and W. S. Stiles, *Color Science: Concepts and Methods, Quantitative Data and Formulas*. New York, NY, USA: Wiley, 1982.
[26] M. Pharr, W. Jakob, and G. Humphreys, *Physically Based Rendering: From Theory to Implementation*. San Mateo, CA, USA: Morgan Kaufmann, 2016.
[27] B. Engquist and A. Majda, "Absorbing boundary conditions for numerical simulation of waves," *Proc. Nat. Acad. Sci.*, vol. 74, no. 5, pp. 1765–1766, May 1977.
[28] N. Okada and J. B. Cole, "Nonstandard finite difference time domain algorithm for Berenger's perfectly matched layer," *Appl. Comput. Electromagn. Soc.*, vol. 26, no. 2, p. 153, 2011.
[29] D. G. Stavenga, "Thin film and multilayer optics cause structural colors of many insects and birds," *Mater. Today, Proc.*, vol. 1, pp. 109–121, 2014.
[30] M. Oren and S. K. Nayar, "Generalization of Lambert's reflectance model," in *Proc. 21st Annu. Conf. Comput. Graph. Interact. Techn.*, 1994, pp. 239–246.
[31] G. Wyszecki, V. S. Stiles, and K. L. Kelly, "Color science: Concepts and methods, quantitative data and formulas," *Phys. Today*, vol. 21, no. 6, pp. 83–84, Jun. 1968.
[32] M. R. Luo, G. Cui, and B. Rigg, "The development of the CIE 2000 colour-difference formula: CIEDE2000," *Color Res. Appl.*, vol. 26, no. 5, pp. 340–350, 2001.
[33] D. L. MacAdam, "Visual sensitivities to color differences in daylight," *J. Opt. Soc. Amer.*, vol. 32, no. 5, pp. 247–274, May 1942.

ZHUO HOU (Member, IEEE) received the M.S. degree in computer science from the University of Tsukuba, Japan, in 2020, where he is currently pursuing the Ph.D. degree with the Graduate School of Systems and Information Engineering. His research interests include computer graphics, structural color, and the design and implementation of electromagnetic simulation models.

DONGSHENG CAI received the B.S. degree in aeronautics from The University of Tokyo, Tokyo, Japan, in 1983, and the M.S. and Ph.D. degrees in electrical engineering from Stanford University, USA, in 1984 and 1989, respectively. He has held positions as a Visiting Professor with the University of California at Los Angeles, from 1994 to 1995; and an Invited Fellow with French National Centre for Scientific Research, from 2001 to 2002. Since 1997, he has been with the University of Tsukuba, Japan. His current research interests include aerospace engineering, space and upper atmospheric physics, color science, visualization, and nonlinear sciences. He is the author of seven books and the author of about 240 publications on these topics. He was a recipient of several awards and distinctions from Centre National de la Recherche Scientifique (CNRS) and the Telecommunications Advancement Foundation. He was a recipient of the Oscar Buneman Award for his pioneering research at the numerical simulation of plasmas.

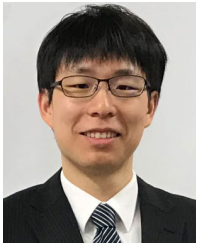

RAN DONG (Member, IEEE) received the Ph.D. degree in engineering, a major in computer science, from the Graduate School of Systems and Information Engineering, University of Tsukuba, in 2020. He is currently a Lecturer with the School of Engineering, Chukyo University, Japan. His research interests include human–machine interaction, numerical simulation, and data analysis. He is also working on projects relating to motion design using deep learning.